Optics Communications 308 (2013) 54–63

Contents lists available at ScienceDirect

Optics Communications

journal homepage: www.elsevier.com/locate/optcom

Effects of plasma confinement on the femtosecond laser ablation of silicon

Chengyun Zhang [a,b], Jianwu Yao [a], Sheng Lan [a,*], Vyacheslav A. Trofimov [c], Tatiana M. Lysak [c]

[a] Laboratory of Nanophotonic Functional Materials and Devices, School of Information and Optoelectronic Science and Engineering, South China Normal University, Guangzhou 510006, China
[b] School of Physics and Electronic Engineering, Guangzhou University, Guangzhou 510006, China
[c] Department of Computational Mathematics and Cybernetics, M. V. Lomonosov Moscow State University, Moscow 119992, Russia

ARTICLE INFO

Article history:
Received 10 March 2013
Received in revised form
25 May 2013
Accepted 18 June 2013
Available online 6 July 2013

Keywords:
Laser ablation
Microstructure fabrication
Laser materials processing
Laser shock processing

ABSTRACT

We investigated the femtosecond laser ablation of silicon in a confined condition by covering the surface of a silicon wafer with a glass slide. The ablation was carried out by either irradiating the focused spot with different numbers of pulses or by scanning the laser beam on the surface of the silicon wafer. The morphology of the ablated surface was characterized by scanning electron microscope. For laser fluences much larger than the ablation threshold of silicon, cylindrical holes were generated in the confined ablation, in sharp contrast to the conical holes observed in the ablation performed in open air. Accordingly, grooves with U-shaped and V-shaped cross sections were achieved in the ablations carried out in the confined condition and in open air, respectively. For laser fluences close to the ablation threshold of silicon, the difference in the morphology of micro- and nanostructures obtained by these two ablation methods became not pronounced and two-dimensional nanohole arrays were created on the surface of silicon wafer. While the period of the nanohole arrays in the direction of the laser polarization was found to be close to the laser wavelength, the period in the direction perpendicular to the laser polarization was observed to be more than two times of the laser wavelength. In addition, the distribution of erupted nanoparticles was also found to be different in the two ablation processes. A ring-shaped distribution of nanoparticles was observed in the open air ablation while a monotonic decrease of nanoparticle density along the radial direction was found in the confined ablation.

1. Introduction

In the last several decades, pulsed laser ablation and deposition have been widely applied in various fields of science and technology [1–5]. In this case, a laser beam with a high peak power is focused on the surface of a material, leading to the ablation of the material which is generally accompanied with the expansion of plasma (plume). The ablation can be carried out in vacuum [6], in air [7], in chemical vapors [8] and even in water [9]. The expanded plasma can be transferred to a receiving substrate that is placed nearby, forming nanoparticles or thin films [2,5]. In particular, laser-induced forward transfer (LIFT) and laser-induced backward transfer (LIBT) have been developed as two special deposition techniques [5,10–14]. In the former case, the laser light is incident from the uncoated side of the transparent substrate and focused at the interface between the substrate and the thin film coated on it. The ejected nanoparticles are deposited on the receiving wafer just behind the film. Thus, it is required that the ablated material should be a thin film coated on a transparent substrate. In the latter case, the laser light is focused on a target film after passing through a transparent substrate. Nanoparticles ejected from the target film are deposited on the substrate. Hence, there is no special requirement for the ablated material. Both LIFT and LIBT technology have been applied in the fabrication of waveguides [15] and nanoparticles [14,16] as well as in the fields of display and biosensing [16,17].

So far, pulsed laser ablation and deposition have been carried out in different environments. In the LIFT and LIBT techniques mentioned above, a dielectric medium is generally employed to confine the expansion of the plasma generated by laser ablation. In these cases, the temperature and pressure resulting from the ablation are much higher than those achieved in the direct ablation without confinement (e.g., in vacuum or in open air). As a result, the micro- and nanostructures created by pulsed laser ablation are expected to be different. Some initial studies have been carried out and the difference in the morphology of the induced micro- and nanostructures was identified [14,18]. It was suggested that the multiple reflection of the laser light between the target and the glass cover and the backward bombardment by the confined plume were

* Corresponding author. Tel.: +86 20 39310378; fax: +86 20 39310309.
E-mail address: slan@scnu.edu.cn (S. Lan).

0030-4018/$ - see front matter © 2013 Elsevier B.V. All rights reserved.
http://dx.doi.org/10.1016/j.optcom.2013.06.052

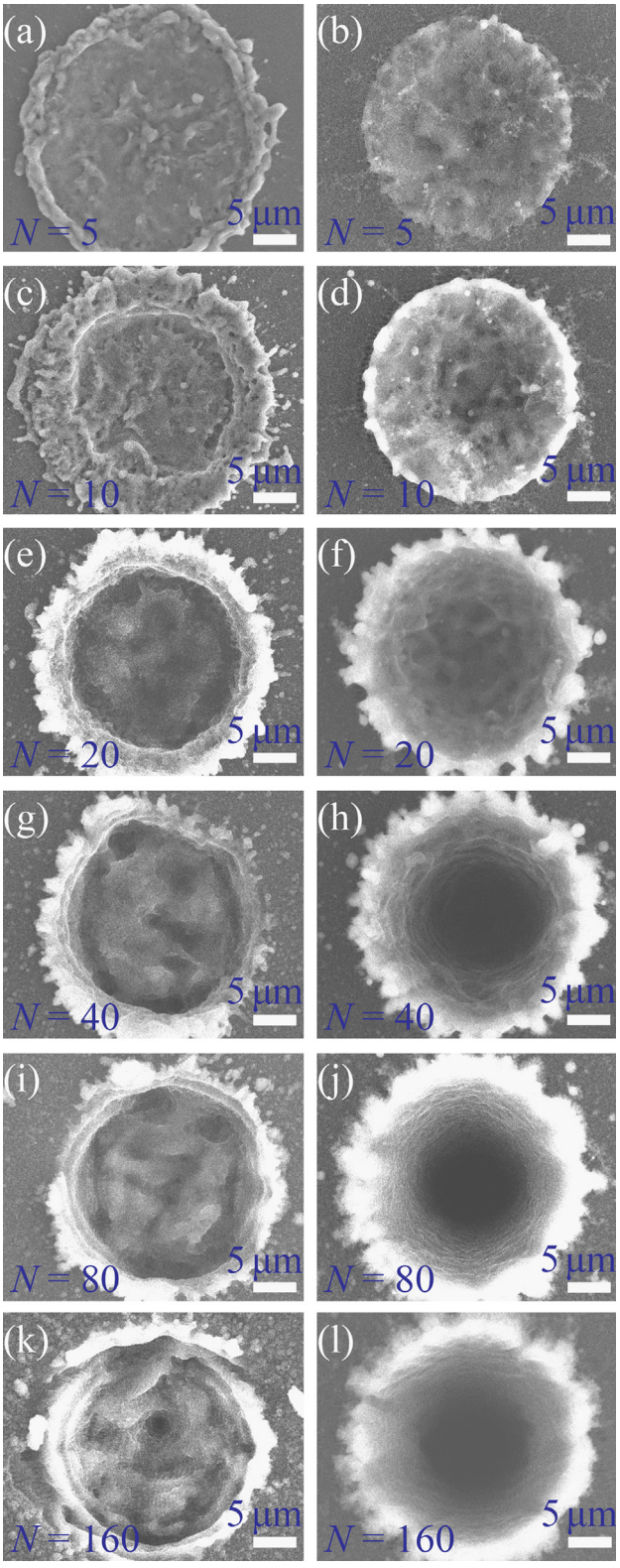

Fig. 1. Comparison of the micrometer-sized holes created in the confined ablation (left column) and in the open-air ablation (right column) for different numbers (N) of irradiated pulses ranging from 5 to 160. The laser fluence was chosen to be 1.114 J/cm^2, which is much larger than the ablation threshold of silicon.

responsible for the change in the morphology [14]. Very recently, the possibility to generate sub-TPa pressure was demonstrated in a confined ablation at the interface between silicon (Si) and silicon oxide (SiO_2) [19]. Since the experimental studies of ionization wave propagation require precise positioning of the laser energy deposition in confined microexplosion conditions, a Si wafer with a thermally oxidized transparent SiO_2 layer on the surface was employed as a target. However, a systematic investigation on the fs laser ablation in a confined condition is still lacking. Actually, there exist two shock waves that propagate into both the ablated material and the confined medium. The LIFT and LIBT techniques lead to an improvement in the mechanical properties of the ablated material and this technique is now referred to as laser shock processing (LSP) [20–22]. In order to utilize only the mechanical effect of the shock wave while avoiding the thermal effect, an absorptive thin film is usually deposited on the material to be processed. For this reason, the effect of the shock wave on the ablation of the material has not been studied, especially in the case when a femtosecond (fs) laser is employed because nanosecond (ns) lasers are generally used in LSP.

In this article, we investigated the ablation of Si in a confined condition by using fs laser pulses. The ablation was carried out by either irradiating the focused spot with different numbers of pulses or by scanning the laser beam on the surface of the Si wafer. The morphology of the micro- and nanostructures generated in the confined ablation is compared in detail with that observed in the ablation performed in open air. The effects of laser fluence on the morphology of the generated micro- and nanostructures were also clarified for laser fluences much larger or just above the ablation threshold of Si.

2. Experimental

The Si wafer used in our experiments was 0.5-mm thick with a surface roughness less than 5 Å. It was n-doped with a resistance less than 0.01 Ω cm. The surface orientation of the Si wafer is (100). A glass slide with a thickness of ~180 μm was chosen as the confining medium because the ablation threshold of glass is much larger than that of Si. It was fixed on the Si wafer with a clamp. When the ablation of Si is carried out at low laser fluence, the nonlinear absorption of glass is negligible and the reduction in laser fluence was caused only by the small reflection of the glass slide. In this case, the thickness of the glass slide does not affect the ablation of Si. In the case of large laser fluence, the reduction in laser fluence originating from the nonlinear absorption will become significant if a thicker glass slide is used. Horizontally-polarized fs pulses delivered by a Ti: sapphire amplifier (Legend, Coherent) was employed in the ablation experiments. The central wavelength, time duration and repetition of the fs pulses were 800 nm, 100 fs, and 1 KHz, respectively. The laser beam was focused on the surface of Si wafer through the glass cover by using a f=150 mm focusing lens, producing a laser spot with a Gaussian profile and a diameter of ~40 μm. The laser fluence was adjusted by using the combination of a waveplate and a polarizer. The ablation was carried out by either irradiating the focused spot with different numbers of pulses or by scanning the laser beam on the surface of the Si wafer. The morphology of the Si surface after fs ablation was examined by using scanning electron microscope (SEM) (S-3700, Hitachi). The depth profiles for the ablated holes and scanned lines were characterized by a surface profilometry (Alpha-Step IQ, KLA-Tencor).

3. Results and discussion

3.1. Micrometer-sized holes created at laser fluences much larger than the ablation threshold of Si

In *fs* laser ablation, a micrometer-sized hole centered at the focused spot is generally created after the ejection of nanoparticles

for laser fluences much larger than the threshold of the ablated material. The appearance of the hole depends strongly on the material properties and the ablation method. The ablation threshold of Si by single fs pulse was reported to be ~0.05 J/cm^2 [6]. In our experiments, we chose a laser fluence of 1.114 J/cm^2, which is much larger than the ablation threshold of Si. A comparison of the micrometer-sized holes generated in the confined and open-air ablations for different numbers of irradiated pulses ranging from 5 to 160 is presented in Fig. 1. Apparently, the major difference between the two cases is the shape of the created holes. It was found that conical holes were formed in the open-air ablation and cylindrical holes were obtained in the confined ablation. Basically, the conical holes observed in the open-air ablation originate from the Gaussian profile of the laser beam. It determines the distribution of temperature and pressure that governs the expansion of plasma and the eruption of nanoparticles. As a result, the ablation is more severe at the center of the laser spot and the holes created in this case usually appear to be conical. In the confined ablation, however, the expansion of plasma is hurdled due to the existence of the confined medium. Consequently, the plasma is confined in a narrow space, leading to a significant enhancement in temperature and pressure and also to a modification of their distribution. In addition, it has been known that the duration of the laser-induced shock wave impacted on the Si will become longer in a confined condition [20]. Furthermore, plastic strain and residual stress fields will be induced if the peak pressure caused by the shock wave exceeds the Hugoniot elastic limit of Si [20,23,24]. All these factors will affect the ablation of Si.

In a confined condition, the maximum pressure induced by laser pulses with a Gaussian profile is proportional to the square root of the laser power density and is independent on the laser pulse duration or laser wavelength [20,24,25]. A peak pressure of ~10 GPa was obtained when the laser power density was chosen to be ~10^9 W/cm^2 [26]. In our case, the peak power density of the *fs* pulses was estimated to be 10^{13} W/cm^2 for an excitation spot diameter of ~40 μm and the resulting peak pressure is much larger than 10 GPa. The Hugoniot elastic limits of Si in the (100), (110), and (111) directions were reported to be 8.4, 5.6, and 5.6 GPa [27,28], respectively. Since the peak pressure generated in the confined ablation is larger than the Hugoniot elastic limit of Si, plastic deformation and strain distribution were induced in the ablation region. The surface roughness and the density of defects are expected to increase, facilitating the subsequent ablation process [20]. More importantly, a compressive stress in the transverse direction was developed in the confined condition, similar to the situation in LSP. This kind of compressive stress, which is schematically depicted in Fig. 2(a), plays a crucial role in the formation of cylindrical holes. From another point of view, the observation of cylindrical holes provides an experimental evidence for the existence of such kind of compressive stress that is previously predicted by theoretical analysis [20]. Another factor that facilitates the formation of cylindrical holes is the modification in the distribution of temperature and pressures. In the confined ablation, the distribution of temperature and pressure over the ablated region will become relatively uniform due to the expansion of plasma in the transverse direction, as schematically shown in Fig. 2(b) [13].

Under high laser fluences, the ablation process becomes complicated because of the high temperature and large pressure. Other factors, such as the phase transition of Si from semiconductor to metal which occurs at ~13 GPa, may also influence the ablation process. In this case, a significant reduction in the volume of Si is expected (~22%), leading to the strain between the ablation area and the surrounding region [28]. More experiments are needed to clarify the effects of these phenomena on the ablation process.

For nanosecond lasers, the time scale for plasma expansion is shorter than pulse duration and plasma shielding results in a decrease in the laser energy reaching the target surface. In this case, the laser energy may be lost through absorption, reflection and scattering. The laser energy absorbed by the plasma will generate very high temperatures ($>$ 5000 K) in the plasma and result in shock waves [29]. In open air, this phenomenon does not occur for femtosecond lasers because of their ultrashort pulse durations and the laser energy is deposited in the target without a laser-plasma interaction [30]. In a confined ablation, however, the duration of the laser-induced shock wave will become longer [20]. As a result, the laser-plasma interaction may become significant at high laser fluences, leading to a temperature much higher than that in open air.

3.2. *Scanned lines obtained at laser fluences much larger than the ablation threshold of Si*

We have shown that micrometer-sized holes can be created by irradiating the Si surface with different numbers of fs laser pulses. Holes with conical and cylindrical shapes can be obtained by using ablations carried out in open-air and confined condition, respectively. In order to further confirm the effects of plasma confinement on the morphology of the generated micro- and nanostructures, we have tried to ablate the Si wafer by scanning the laser beam with a fixed laser fluence on the surface. The average number of pulses irradiated on the excitation spot was adjusted by changing the scanning speed of the laser beam. The SEM images of the scanned lines obtained at different scanning speeds by using the two ablation methods are compared in Fig. 3. It can be clearly seen that scanned lines with V-shaped cross sections are generated in the open-air ablation while the scanned lines formed in the confined ablation possess U-shaped cross sections. In both cases, the depth of the scanned lines increases with decreasing scanning speed. The V-shaped and U-shaped cross sections of the scanned lines are in accordance with the conical and cylindrical holes achieved in the two ablation processes.

In order to get the cross sections of the formed holes and grooves, we have performed atomic force microscope (AFM) measurements on the holes and grooves. Unfortunately, the depths of the holes and grooves exceed the measurement limit of the AFM in the vertical direction which is only 5 μm. In order to clearly show the morphology of the ablated region, we provide the

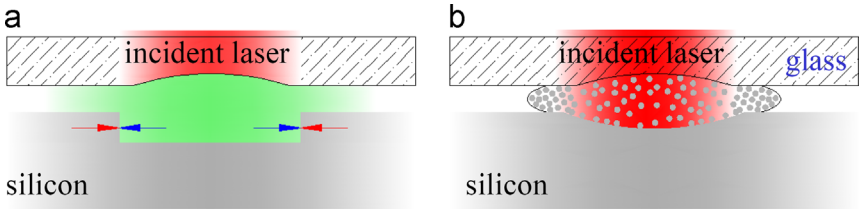

Fig. 2. (a) Schematic presentation of the compressive residual stresses generated by laser-induced shock wave in the confined ablation. The blue and red arrows indicate the compressive residual stresses during and after the interaction and the shock wave is represented by green color. (b) Schematic of the expansion of plasma in the transverse direction due to the existence of the confinement. (For interpretation of the references to color in this figure legend, the reader is referred to the web version of this article.)

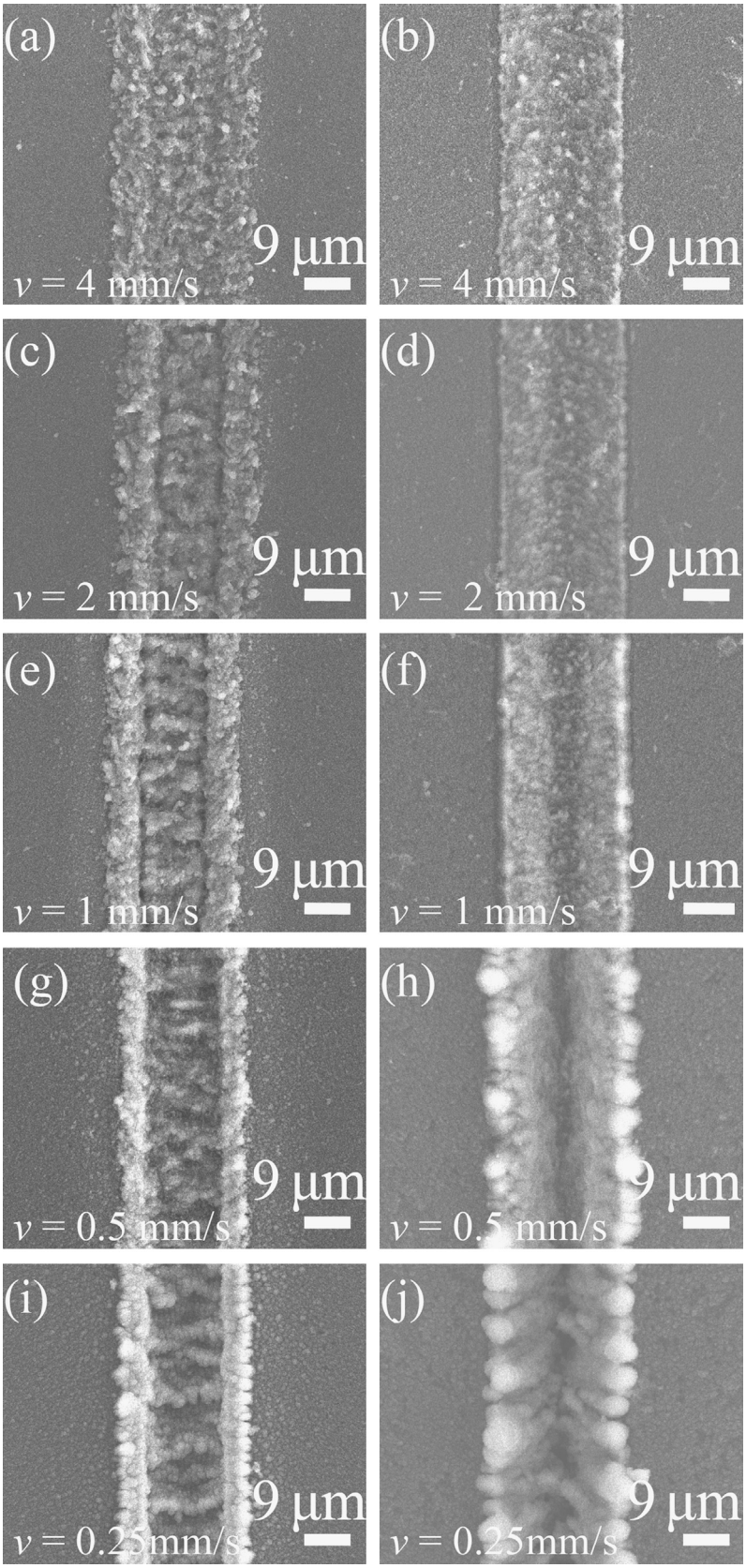

Fig. 3. Comparison of the scanned lines obtained at different scanning speeds by using the confined ablation (left column) and the open-air ablation (right column).

SEM images of the holes and grooves taken at an angle of 10°, as shown in Fig. 4. Previously, Mizeikis et al. used HF water solution to remove the Si/SiO_2 debris distributed on the surface of the Si wafer in order to see the underneath morphology of the ablated holes [31]. In our case, we removed such Si/SiO_2 debris by ultrasonic cleaning for SEM observation and depth profile measurement, as shown in Fig. 4(b). Some ripples were found on the surface near the ablated holes.

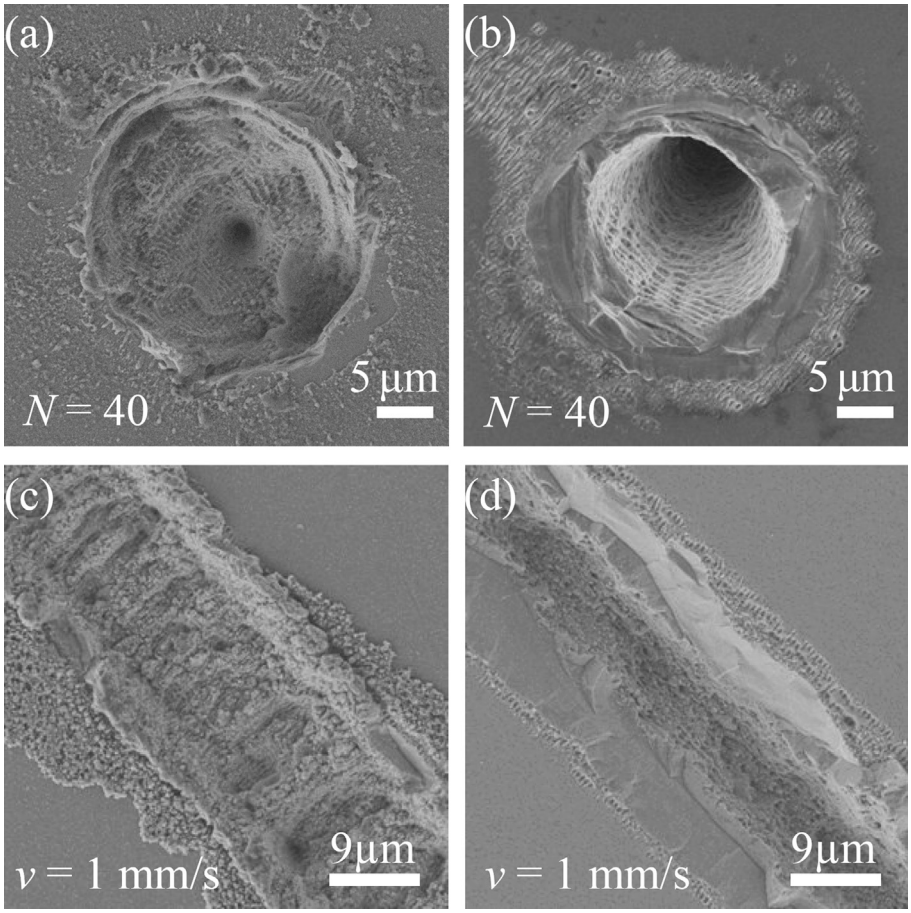

Fig. 4. Comparison of the holes and grooves obtained by using the confined ablation (left column) and the open-air ablation (right column). The SEM images were taken at an angle of 10°. The holes shown in (a) and (b) correspond to those shown in Fig. 1(g) and (h) while the grooves shown in (c) and (d) correspond to those shown in Fig. 3 (e) and (f). The nanoparticles accumulated at the edges of the holes and grooves have been removed by ultrasonic cleaning.

In order to show more clearly the cross section of the ablated holes and scanned lines, we employed a surface profilometry to measure the depth profiles of the ablated holes and the scanned lines shown in Fig. 4. The measurement results are presented in Fig. 5. The depth profiles clearly indicate the creation of cylindrical holes and U-shaped grooves in the confined ablation and the formation of conical holes and V-shaped grooves in the open air ablation.

3.3. *Micro- and nanostructures created at laser fluences just above the ablation threshold of Si*

As mentioned above, the ablation of Si with laser fluences much larger than the ablation threshold of Si is rather complicated because plastic strain and stress fields are induced by the shock wave generated in the ablation. It has been shown that a peak pressure exceeding the Hugoniot elastic limit of Si can be easily achieved by using the confined ablation. As a systematic investigation of confined ablation, it is interesting to find out the effects of laser fluence on the morphology of the micro- and nanostructures created in the two ablation methods. For this reason, we have tried to ablate the Si with a laser fluence of 148 mJ/cm^2, just above the ablation threshold of Si. The micro- and nanostructures obtained by using the two ablation methods are compared in Fig. 6 for different numbers of irradiated pulses. In both cases, the generated micro- and nanostructures are found to be much different from those observed at high laser fluences.

When the number of irradiated pulses is small ($N=10$), one can identify ripples with a subwavelength period appearing at the edge of the ablation region. At the center of the ablation region, these ripples are smeared and replaced by arrays of nanoholes. A clearer image of such ripples, which was obtained with a smaller number of irradiated pulses ($N=5$), is shown in the inset of Fig. 6(b). Recently, we have reported the formation of regular nanohole arrays on the surface of Si by using fs laser ablation [32]. The physical mechanism that is responsible for the transition from ripples to nanohole arrays was interpreted as the redistribution of the electric field on the surface induced by the formation of ripples. In addition, we have successfully explained the formation of high spatial frequency periodic surface structure on metal surface by using this physical mechanism [33].

In practice, regular nanohole arrays can be achieved by scanning the laser beam with appropriate laser fluence and scanning speed on the surface of Si. If laser pulses are continuously irradiated on the same point, the nanohole arrays will be preferentially created at the center of the laser spot where the length of ripples exceeds the critical value for the formation of nanoholes. In a previous study, we have shown by numerical simulation that the first maximum of electric field begins to appear in the grooves when the length of the grooves exceed a critical value of ~4 μm [32]. It was found that the length and depth of initially formed grooves are crucial for the generation of nanohole arrays. For short and shallow grooves, the electric field was concentrated at the center of each groove. Consequently, the subsequent ablation occurred preferentially at the center of each groove, leading to the formation of a nanohole chain. For larger laser fluences, it was expected that deeper and longer grooves would be created on the surface. In this case, the number of the maximums in the electric field distribution increased and a nanohole array was achieved.

At the edge of the laser spot where the ripples are shallow, no nanohole was generated. That is the phenomenon we observed in the

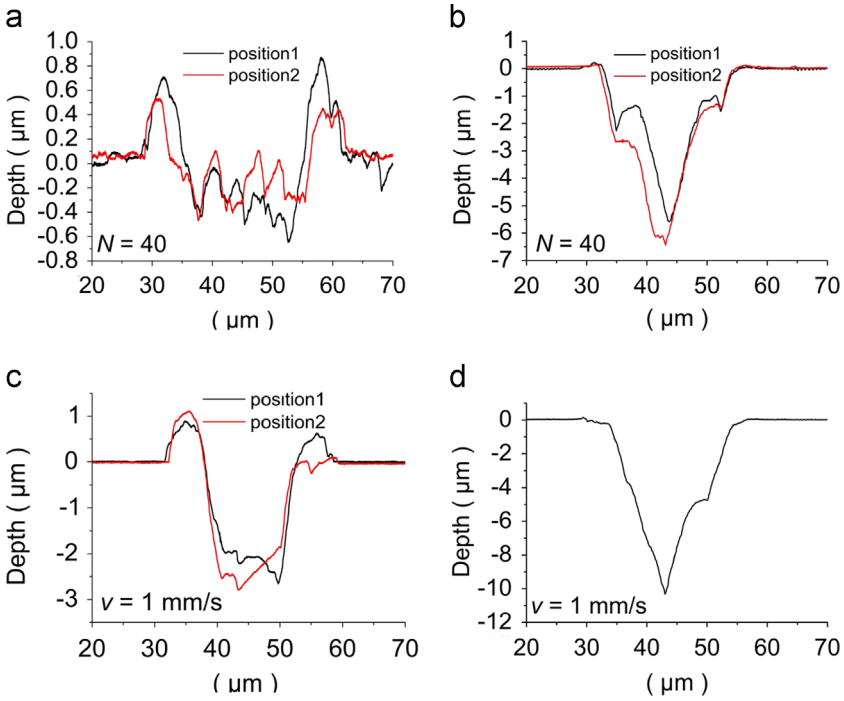

Fig. 5. Profile comparison of the holes and grooves obtained in the confined ablation (left column) and in the open-air ablation (right column) for pulse numbers $N=40$ and scanning speeds $v=1$ mm/s. The holes shown in (a) and (b) correspond to those shown in Fig. 4(a) and (b) while the grooves shown in (c) and (d) correspond to those shown in Fig. 4(c) and (d). The laser fluence was chosen to be 1.114 J/cm^2, which is much larger than the ablation threshold of silicon.

experiments. For the ablation in open-air, it is noticed that the nanoholes created at the center of the ablation region disappeared when the number of irradiated pulses was increased to $N=20$. It is because the ablation is more severe at the center. The nanoholes located at the edge of the ablation region were left unmodified. A conical hole was gradually formed with increasing number of irradiated pulses although its shape is not as regular as that observed at high laser fluences. In comparison, the nanoholes located at the center of the ablation region were maintained in the confined ablation for a large number of irradiated pulses of $N=160$. They disappeared completely at $N=1000$. We think that this feature is a benefit from the relatively uniform spatial distribution of temperature and pressure over the ablation region caused by plasma confinement.

In Fig. 6, it is also noticed that ablation region in the open-air condition is larger than that in the confined condition. Since the laser fluence used in both cases was same, it is thought that the reflection of the glass cover reduces, to some extent, the laser fluence. As a result, the laser fluence after passing through the glass cover becomes smaller than the ablation threshold of Si. Fortunately, the reduction in laser fluence is partly compensated by the enhancement in temperature and pressure induced by plasma confinement. It should be emphasized that the effects of confinement are not significant for low laser fluences because the expansion of plasma and the eruption of nanoparticles are not pronounced. Therefore, similar appearance and evolution of the generated micro- and nanostructures are observed in the two ablation processes.

The plasma confinement affects the ablation process in a completely different way when the laser fluence employed in the ablation is just above the ablation threshold. In this case, ripples are created after irradiating a few laser pulses when the expansion of plasma is almost negligible. Consequently, the difference between the ablation in a confined condition and that in open air is not obvious. After the formation of ripples or even nanohole arrays, however, strong localization of electric field in these nanostructures leads to severe ablation and nanoparticle eruption. At this stage, the confinement of plasma becomes effective and it results in uniform distributions of temperature and pressure. As a result, the nanohole array was maintained for a large number of laser pulses ($N=160$), as shown in the inset of Fig. 6(i). In sharp contrast, the nanohole array disappeared at a small number of laser pulses ($N=10$) and a deep conic hole was formed at the center of the ablation region, as shown in the inset of Fig. 6(b).

It is expected that the nonuniform distribution of temperature and pressure on Si surface in the open-air ablation, which is close to the Gaussian profile of the laser beam, can be smeared out in one direction through the scanning of the laser beam. By doing so, a relatively uniform distribution of temperature and pressure can be achieved along the scanned lines. As a result, regular nanohole arrays can be obtained and the difference between the two ablation processes will become less pronounced. The SEM images of the scanned lines generated in the two ablation processes are compared in Fig. 7 for different scanning speeds. It is obvious that similar two-dimensional (2D) nanohole arrays were created in the two ablation processes, indicating that the difference between the two ablation methods has been significantly reduced. While the period of the nanohole arrays in the direction of the laser polarization was found to be close to the laser wavelength, the period in the direction perpendicular to the laser polarization was observed to be more than two times of the laser wavelength (~2 μm), as indicated by the arrow in Fig. 7(b). Previously, Mizeikis et al. observed a square-shaped nanohole array with empty core at the Si–SiO_2 interface [31]. In addition, Buividas et al. found that the spatial period for the ripples formed on semiconductors was determined to be $\lambda/2n$, where is the laser wavelength in vacuum and n is the refractive index of the material [34]. By optimizing the laser fluence and scanning speed, 1D nanohole chains and 2D nanohole arrays with regularly arranged nanoholes could be obtained [32]. Therefore, it is concluded that the confinement plays less important role in the ablation carried at low laser fluences because of the weak or absence of plasma expansion.

In Fig. 7, it is noticed that the 2D nanohole arrays obtained in the open-air ablation appear to be better than those obtained in the confined ablation. It is thought that the ejected nanoparticles are tightly confined in a narrow gap between the Si wafer and the

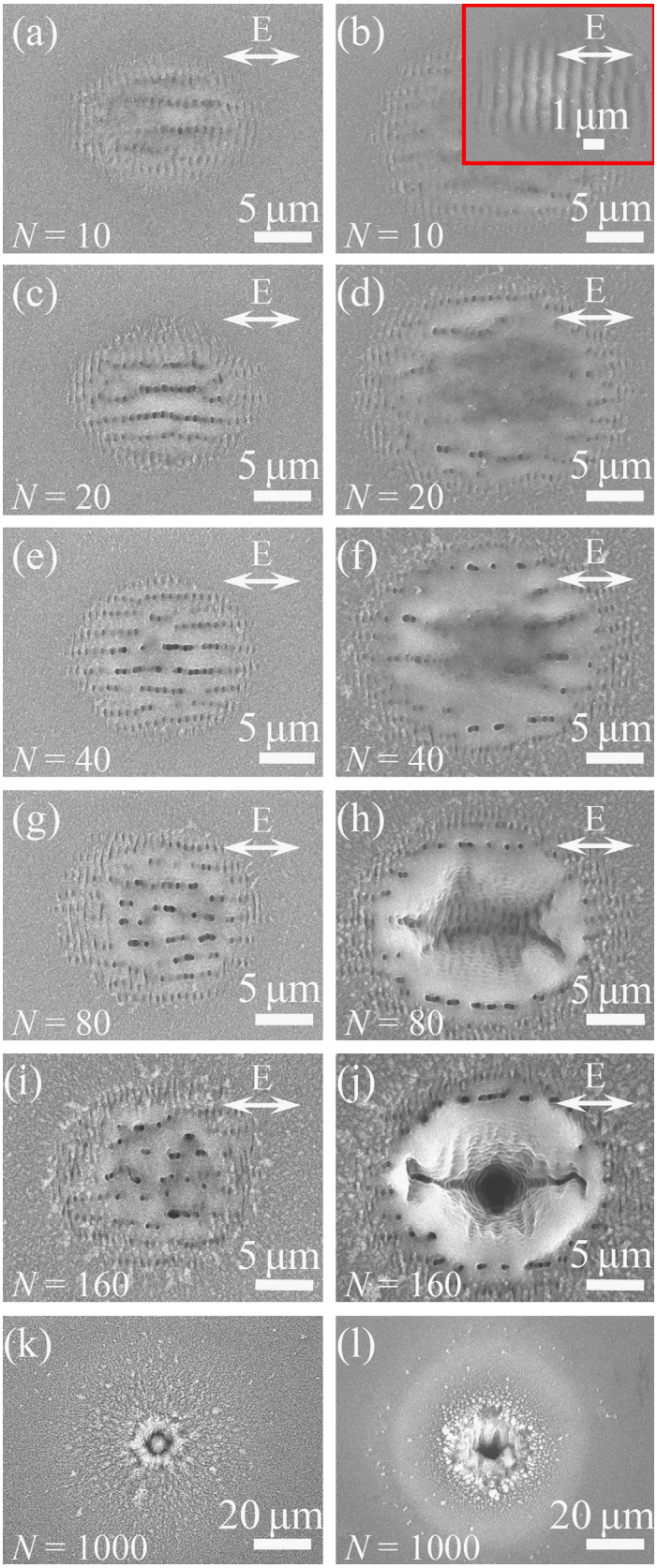

Fig. 6. Comparison of the micro- and nanostructures created in the confined ablation (left column) and in the open-air ablation (right column) for different numbers of irradiated pulses ranging from 10 to 1000. The laser fluence was chosen to be 148 mJ/cm^2, which is just above the ablation threshold of silicon.

glass slide in the confined ablation. As a result, the scattering, absorption and redistribution of the laser light by these nanoparticles will affect the subsequent ablation process.

Apart from the difference in the morphology of the generated micro- and nanostructures discussed above, there also exists a difference in the distribution of the erupted nanoparticles, as can

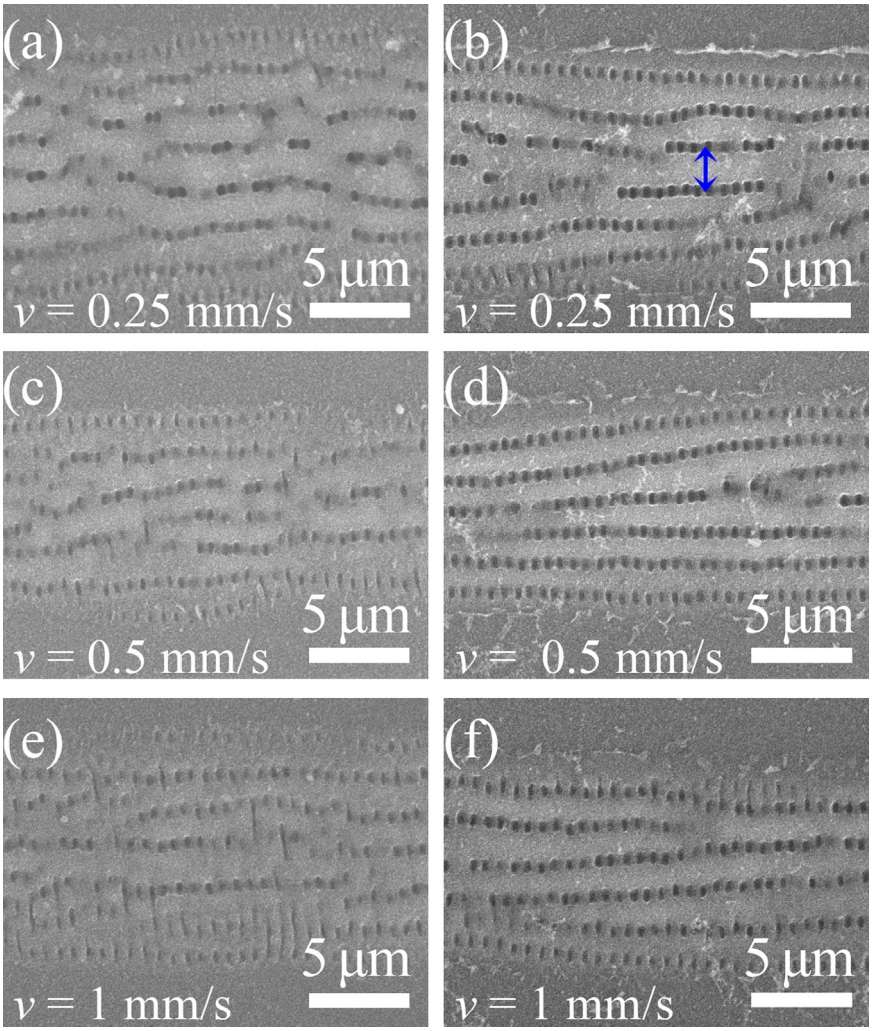

Fig. 7. Comparison of the scanned lines obtained at different scanning speeds by using confined ablation (left column) and the open-air ablation (right column). The laser fluence was chosen to be 148 mJ/cm^2, which is just above the ablation threshold of silicon.

be seen in Fig. 6(k) and (l). In the open-air ablation, nanoparticles erupt along the normal of the Si surface, forming a ring-shaped distribution. Differently, a radial distribution of the erupted nanoparticles is observed in the confined ablation due to the existence of confinement in the eruption direction. A comparison of the distribution of nanoparticles obtained by using the two ablation methods for different numbers of irradiated pulses is presented in Fig. 8. In the open-air ablation, the erupted nanoparticles exhibit a ring-shaped distribution circling the central hole, as can be seen in the right column of Fig. 8. The diameter of the ring was estimated to be ~100 μm. The distribution of nanoparticles around the ring appears to be broad for numbers of irradiated pulses (N=5, 10). With increasing number of irradiated pulses (N=20), the distribution of nanoparticles around the ring becomes narrower. In the confined ablation, the situation is completely different. For numbers of irradiated pulses (N=5, 10, and 20), the density of erupted nanoparticles exhibits a monotonic decrease along the radial direction, as shown in Fig. 8(a), Fig. 3(c) and (e). However, the diameter of the ring appeared to be smaller (~80 μm) in this case.

We think that the distribution of erupted nanoparticles is mainly governed by the expansion of plasma. In the open-air ablation, the eruption of nanoparticles originate from the Gaussian profile of the laser beam. It determines the distribution of temperature and pressure that governs the expansion of plasma and the eruption of nanoparticles. Thus, the ring-shaped distribution of nanoparticles is easily understood. For the confined ablation, most erupted nanoparticles were deposited on the glass cover and it forms the basis of LIBT. Therefore, it can be seen in Fig. 8 that the density of nanoparticles distributed on the Si surface is smaller than that achieved in the open-air ablation. In addition, the expansion of plasma in the transverse direction will modify the way nanoparticles erupt, leading to the distribution of nanoparticles that decreases almost monotonically along the radial direction observed in the experiments.

It has been demonstrated that the confinement of plasma plays a crucial role in the LIFT and LIBT techniques by which the distribution of erupted nanoparticles can be controlled. Previously, the LIBT technique was employed by Liu et al. to realize continuous variation of gray scale bitmap images and phosphorescent images [13,14]. In addition, these techniques can be employed to fabricate surface channels for microfluid and waveguides. Furthermore, the cylindrical holes and U-shaped grooves obtained in the confined ablation further confirms the existence of the stress perpendicular to the laser light predicted in the LSP [20], providing a way for exerting stress on the target material in the LSP.

4. Conclusion

We have investigated the effects of plasma confinement on the ablation of Si by covering the Si surface with a glass slide. For fs laser ablation carried out at laser fluences much larger than the ablation

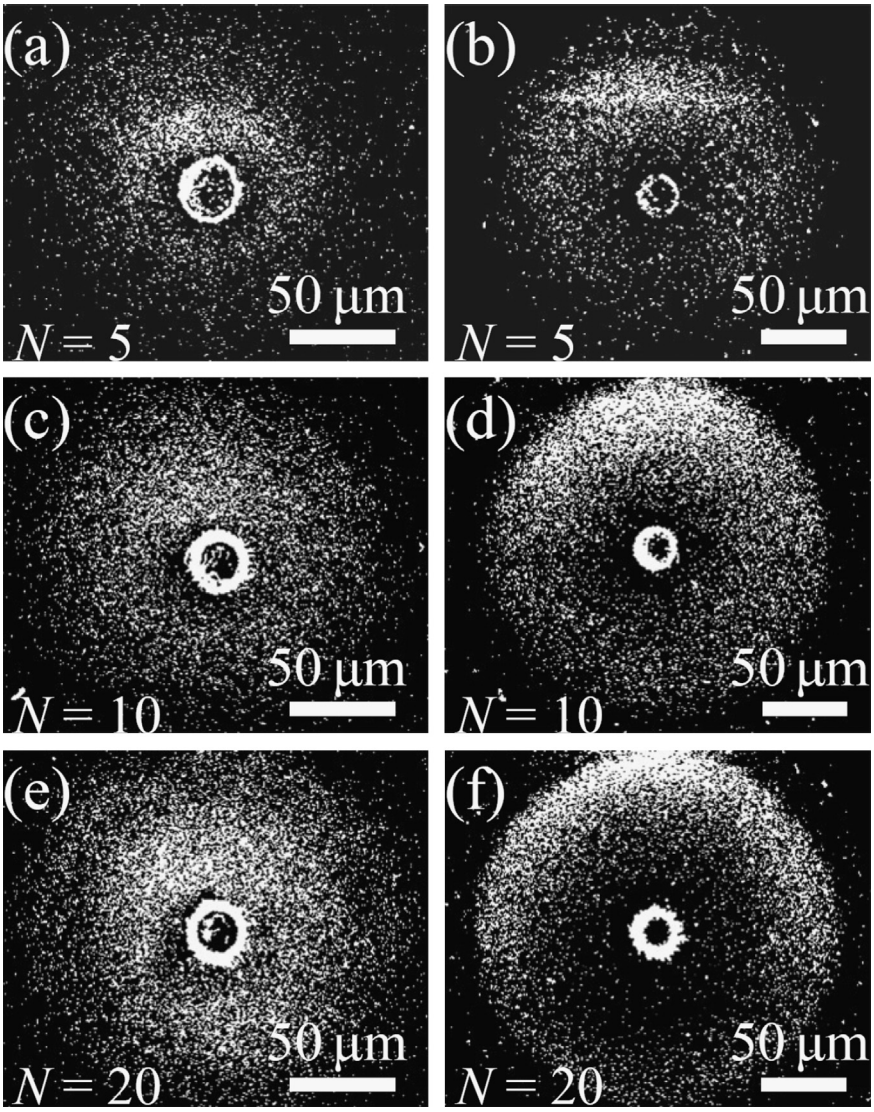

Fig. 8. Comparison of the distribution of nanoparticles obtained by using the confined ablation (left column) and in the open-air ablation (right column) for different numbers of irradiated pulses ranging from 5 to 20. The contrasts of the images have been enhanced in order to clearly show the distribution of the erupted nanoparticles on the silicon surface. The laser fluence was chosen to be 1.114 J/cm^2, which is much larger than the ablation threshold of silicon.

threshold of Si, it was found that cylindrical holes and U-shaped lines were created in the confined ablation when irradiating the focused spot with fs laser pulses or scanning the laser beam on the Si surface. In comparison, conical holes and V-shaped lines were observed in the open-air ablation. For laser fluences just above the ablation threshold of Si, the difference in the morphology of micro- and nanostructures obtained by these two ablation methods became not pronounced. In this case, 2D nanohole arrays were created by either irradiating the focused spot with different number of pulses or scanning the laser beam on the Si surface. While the period of the nanohole arrays in the direction of the laser polarization was found to be close to the laser wavelength, the period in the direction perpendicular to the laser polarization was observed to be more than two times of the laser wavelength. The distribution of erupted nanoparticles was also found to be different in the two ablation processes. While a ring-shaped distribution of nanoparticles was observed in the open air ablation, a monotonic decrease of nanoparticle density along the radial direction was found in the confined ablation. The results presented in this work are helpful for the use of confined ablation in the fabrication of micro- and nanostructures.

Acknowledgments

The authors acknowledge the financial support from the National Natural Science Foundation of China (Grant nos. 10974060, 51171066 and 11111120068) and the program for high-level professionals in the universities of Guangdong province, China.

References

[1] D. Vipparty, B. Tan, K. Venkatakrishnan, Journal of Applied Physics 112 (2012) 073109-1.
[2] M.N.R. Ashfold, F. Claeyssens, G.M. Fuge, S.J. Henley, Chemical Society Reviews 33 (2004) 23.
[3] S. Noël, J. Hermann, T. Itina, Applied Surface Science 253 (2007) 6310.
[4] S. Amoruso, G. Ausanio, R. Bruzzese, M. Vitiello, X. Wang, Physical Review B 71 (2005) 033406.
[5] A.I. Kuznetsov, J. Koch, B.N. Chichkov, Optics Express 17 (2009) 18820.
[6] A.Y. Vorobyev, C. Guo, Applied Physics Letters 86 (2005) 011916.
[7] A.Y. Vorobyev, C. Guo, Optics Express 14 (2006) 2164.
[8] T.H. Her, R.J. Finlay, C. Wu, S. Deliwala, E. Mazur, Applied Physics Letters 73 (1998) 1673.

[9] R. Intartaglia, K. Bagga, F. Brandi, G. Das, A. Genovese, E. Di Fabrizio, A. Diaspro, Journal of Physical Chemistry C 115 (2011) 5102.
[10] C. Boutopoulos, E. Touloupakis, I. Pezzotti, M.T. Giardi, I. Zergioti, Applied Physics Letters 98 (2011) 093703.
[11] L. Yang, C.Y. Wang, X.C. Ni, Z.J. Wang, W. Jia, L. Chai, Applied Physics Letters 89 (2006) 161110.
[12] D.A. Willis, V. Grosu, Applied Physics Letters 86 (2005) 244103.
[13] B. Liu, Z. Hu, M. Murakami, J. Xu, Y. Che, Pulsed laser micro-deposition pattern formation, IMRA AMERICA Inc., US Patent 0227133 A1, 2010.
[14] B. Liu, Z. Hu, Y. Che, Proceedings of the SPIE 7590 (2010) 759002.
[15] K.S. Kaur, A.Z. Subramanian, Y.J. Ying, D.P. Banks, M. Feinaeugle, P. Horak, V. Apostolopoulos, C.L. Sones, S. Mailis, R.W. Eason, Optics Express 19 (2011) 9814.
[16] J.M. Fitz-Gerald, A. Piqué, D.B. Chrisey, P.D. Rack, M. Zeleznik, R.C.Y. Auyeung, S. Lakeou, Applied Physics Letters 76 (2000) 1386.
[17] P. Serra, J.M. Fernández-Pradas, M. Colina, M. Duocastella, J. Domínguez, J.L. Morenza, Journal of Laser Micro/Nanoengineering 1 (2006) 236.
[18] J. Bohandy, B.F. Kim, F.J. Adrian, Journal of Applied Physics 60 (1986) 1538.
[19] E.G. Gamaly, L. Rapp, V. Roppo, S. Juodkazis, A.V. Rode, New Journal of Physics 15 (2013) 025018.
[20] P. Peyre, R. Fabbro, Optical and Quantum Electronics 27 (1995) 1213.
[21] V.I. Mazhukin, V.V. Nossov, I. Smurov, Journal of Applied Physics 90 (2001) 607.
[22] G. Gomez-Rosas, C. Rubio-Gonzalez, J.L. Ocaña, C. Molpeceres, J.A. Porro, W. Chi-Moreno, M. Morales, Applied Surface Science 252 (2005) 883.
[23] W. Zhang, Y.L. Yao, Journal of Manufacturing Science and Engineering 124 (2002) 369.
[24] A.H. Clauer, J.H. Holbrook, B.P. Fairand, Shock Waves and High-Strain-Rate Phenomena in Metals, Plenum Press, New York675–697.
[25] R. Fabbro, J. Fournier, P. Ballard, D. Devaux, J. Virmont, Journal of Applied Physics 68 (1990) 775.
[26] B.P. Fairand, A.H. Clauer, Journal of Applied Physics 50 (1979) 1497.
[27] M.C. Gupta, A.L. Ruoff, Journal of Applied Physics 51 (1980) 1072.
[28] T. Goto, T. Sato, Y. Syono, Japanese Journal of Applied Physics 21 (1982) L369.
[29] D.X. Hammer, E.D. Jansen, M. Frenz, G.D. Noojin, R.J. Thomas, J. Noack, A. Vogel, B.A. Rockwell, A.J. Welch, Applied Optics 36 (1997) 5630.
[30] X. Zeng, X.L. Mao, R. Greif, R.E. Russo, Applied Physics A 80 (2005) 237.
[31] V. Mizeikis, S. Juodkazis, J. Ye, A. Rode, S. Matsuo, H. Misawa, Thin Solid Films 438–439 (2003) 445.
[32] C.Y. Zhang, J.W. Yao, H.Y. Liu, Q.F. Dai, L.J. Wu, S. Lan, V.A. Trofimov, T.M. Lysak, Optics Letters 37 (2012) 1106.
[33] J.W. Yao, C.Y. Zhang, H.Y. Liu, Q.F. Dai, L.J. Wu, S. Lan, A.V. Gopal, V.A. Trofimov, T.M. Lysak, Optics Express 20 (2012) 905.
[34] R. Buividas, L. Rosa, R. Šliupas, T. Kudrius, G. Šlekys, V. Datsyuk, S. Juodkazis, Nanotechnology 22 (2011) 055304.